LAWRENCE
LIVERMORE
NATIONAL
LABORATORY

LLNL-CONF-488654

Compact Linear Accelerator Sources for Gamma-ray Generation

S. G. Anderson, C. P. Barty, G. Beer, R. R. Cross, C. A. Ebbers, D. J. Gibson, F. V. Hartemann, T. L. Houck, R. A. Marsh, C. Adolphsen, T. S. Chu, E. N. Jongewaard, Z. Li, C. Limborg-Deprey, T. O. Raubenheimer, S. G. Tantawi, A. E. Vlieks, W. J. Wang

June 17, 2011

Institute of Nuclear Materials Management 52nd Annual Meeting
Palm Desert, CA, United States
July 17, 2011 through July 22, 2011

Disclaimer

Compact Linear Accelerator Sources for Gamma-ray Generation

S.G. Anderson, C.P.J. Barty, G. Beer, R.R. Cross, C. A. Ebbers,
D.J. Gibson, F.V. Hartemann, T. Houck, and R. A. Marsh
Lawrence Livermore National Laboratory
7000 East Avenue, Livermore, CA 94550

C. Adolphsen, T.S. Chu, E.N. Jongewaard, Z. Li, C. Limborg-Deprey,
T. Raubenheimer, S.G. Tantawi, A. Vlieks, and J.W. Wang
SLAC National Accelerator Laboratory
2575 Sand Hill Road, Menlo Park, CA 94025

ABSTRACT
High precision accelerator technology is required for the development of tunable, monochromatic gamma-ray sources capable of generating MeV photons with very high brightness. High gradient accelerator technology is capable of producing high brightness electron beams in relatively short lengths. X-band technology has been demonstrated extensively in the development of the Next Linear Collider program at SLAC, and has been adapted for use in a Compton scattering gamma-ray source at LLNL. Critical components and technologies will be discussed including the use of high repetition rate solid state modulators, XL4 klystrons, SLED-II pulse compression, RF distribution geometries, a novel X-band RF photoinjector, high gradient traveling wave accelerator structures, and linear accelerator design and layout. Selection of beam properties relevant to gamma-ray production will be discussed, especially with respect to future improvements in gamma-ray brightness and dose specific to nuclear management applications.

INTRODUCTION
Nuclear Resonance Fluorescence (NRF) [1] is an isotope specific process in which a nucleus, excited by gamma-rays, radiates high energy, narrow bandwidth photons. Because NRF energy levels depend on the exact nuclear structure, the NRF spectrum is isotope-dependent. NRF lines are found in the MeV energy range, where photons are most penetrating, near the absorption minimum between photo-ionization and pair production.

Although NRF is a process that has been well known for several decades, with the advent of Mono-Energetic Gamma-ray (MEGa-ray) sources from Compton scattering, it has now potential high impact applications in homeland security, nuclear waste assay, medical imaging and stockpile surveillance, among other areas of interest. Although several successful experiments have demonstrated NRF detection with broadband bremsstrahlung gamma-ray sources [2], NRF lines are more efficiently detected when excited by narrowband gamma-ray sources. Currently, Compton scattering is the only physical process capable of producing tunable narrow bandwidth radiation (below 1%) at gamma-ray energies, with state-of-the art accelerator and laser technologies. In Compton scattering sources, a short laser pulse and a relativistic electron beam collide to yield tunable, monochromatic, polarized gamma-ray photons. Several projects have recently utilized Compton scattering to conduct NRF experiments: Duke university [3], Japan [4], and Lawrence Livermore National Laboratory (LLNL) [5-7]. In particular, LLNL's Thomson-Radiated Extreme X-rays (TREX) project demonstrated isotope specific detection of low-density materials behind heavier elements [5].

The proposed NRF applications need high average photon flux at a specified energy (i.e., to maximize N_γ / eV / sec at the NRF resonance lines) while concurrently minimizing background noise from off-resonance radiation. For the Compton source, these requirements motivate the use of small laser and electron beam sizes, σ_x, at the interaction point (IP) to increase flux, yet maintain a small normalized beam divergence, $\gamma\sigma_{x'}$, to decrease the bandwidth of the γ-rays. In fact, it can be shown [8] that the accelerator design should seek to maximize the quantity:

$$N_\gamma \,/\, \mathrm{eV} \,/\, \mathrm{sec} \propto \frac{\langle I \rangle}{\varepsilon_n^2},$$

where <*I*> is the average current of the accelerator, and ε_n is the normalized beam emittance.

This paper describes the VELOCIRAPTOR linac (Very Energetic Light for the Observation and Characterization of Isotopic Resonances and the Assay and Precision Tomography of Objects with Radiation), designed to drive a precision, compact, γ-ray source by optimizing $\langle I \rangle / \varepsilon_n^2$. Rf photoinjector and traveling wave linac technology operating at X-band (11.424 GHz) was chosen for this application due to recently demonstrated advancements in accelerating field gradients [9], and the potential for very high brightness beam generation. Below, the photoinjector design, traveling-wave accelerator design, X-band rf compression and distribution systems, and electron beam dynamics simulations will be presented with emphasis given to design requirements imposed by this light source application.

RF PHOTOINJECTOR

The X-band rf photoinjector was based on an earlier design developed by A. Vlieks at SLAC [10,11]. The Vlieks design was the first X-band photoinjector, and was operated successfully at cathode electric fields of 200 MV/m. The Vlieks photoinjector was a 5.5 cell design, and as such

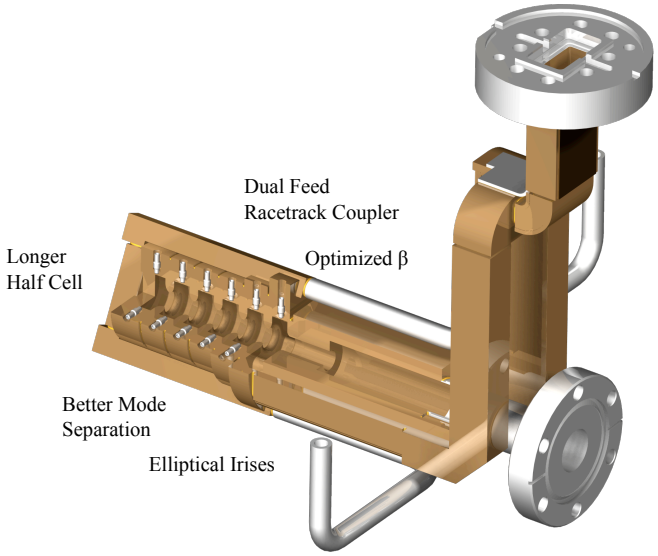

Figure 1. CAD rendering of VELOCIRAPTOR X-band rf photoinjector. Labels indicate major design improvements over the Vlieks design.

supported 6 eigenmodes near the operating p-mode. The mode separation between the operating mode and its nearest neighbor was less than 10 MHz, leading to simultaneous excitation of both modes by the drive rf, resulting in mode beating of the fields on the cathode, and degradation in achievable beam brightness.

The VELOCIRAPTOR photoinjector advances on the Vlieks design by increasing the mode separation to 25 MHz, and incorporates other significant improvements to enhance its robust operation as the VELOCIRAPTOR electron source. A CAD rendering of the photoinjector is shown in Figure 1. The major design changes include: iris geometry change from circular cross-section irises to elliptical contoured; iris thickness adjustment to improve mode separation; a longer initial half cell; a racetrack coupler; and coupling optimization to balance pulsed heating with cavity fill time. A description of the detailed design process and supporting simulations will be presented in [12]. A summary follows, reporting only design achievements. A combination of design codes was used including PARMELA, HFSS, and the ACE3P suite of codes developed at SLAC [13].

Eigenmode excitation modeling showed that the Vlieks design mode separation of 8.7 MHz led to an increase in the photoinjector beam divergence. In order to generate as bright a beam as possible, the mode separation was increased to 25 MHz, at which point mode beating contributed a negligible emittance increase. The final iris parameters were held fixed for the remainder of the design changes, and the mode separation was maintained.

Changing the iris geometry can spread the electric field maximum over a wider surface area, and decrease the peak surface electric field for a given gradient. Following [14], the optimal iris ellipticity is dependent on the exact iris radius and thickness. For the VELOCIRAPTOR design this geometry was fixed by the changes made to improve the mode separation. An improvement of 10% was accomplished in the achieved axial electric field relative to the peak surface field by adopting irises with an elliptical axial contour. The irises remained cylindrically symmetric with respect to the beam axis, the elliptical contour is only visible in their cross-section, e.g. the cutaway in Fig. 1.

The half cell in the Vlieks design photoinjector was slightly under an exact half cell in length. Running beam dynamics simulations to optimize the emittance after compensation, an optimal half cell length was determined.

The coupler for the Vlieks design photoinjector was a dual feed design, but continued to have a small quadrupole component that would increase the head to tail beam asymmetry, and increase the beam emittance. In order to lower this effect to ignorable levels, a racetrack coupler was designed similar to that used in the LCLS injector [15]. The decrease in rf quadrupole between the VELOCIRAPTOR and Vlieks designs is a factor of 100, virtually eliminating this source of emittance growth.

The optimal coupling into the photoinjector is a balance between the power available, the pulse length used, and the resulting pulsed heating. Circuit models were used to determine the balance achievable, and then choose an operating point that is relatively insensitive to fabrication tolerances, and the fact that the ultimate gun coupling will have to be measured and tuned after fabrication.

Water cooling will be accomplished in the same manner as the Vlieks design, with a single brazed water channel. Vacuum will be provided by a circularly symmetric pump-out port on the beamline, and waveguide pump-outs on the feed waveguide. Final electromagnetic design incorporated all of the features described, and achieved a p-mode frequency of 11.424 GHz, a uniform field balance of <1% flatness variation, and a coupling *b* of ~1.7.

LOW ENERGY BEAMLINE

The drift section between the photoinjector and the first accelerator section is critical because it must incorporate the laser input to the cathode, sufficient injector diagnostics, and accommodate the gun solenoid and emittance compensation process. In addition, at low energy care must be taken to minimize the wakefields produced by irregular vacuum chambers. The VELOCIRAPTOR Low Energy Beamline (LEB) design is shown in Figure 2.

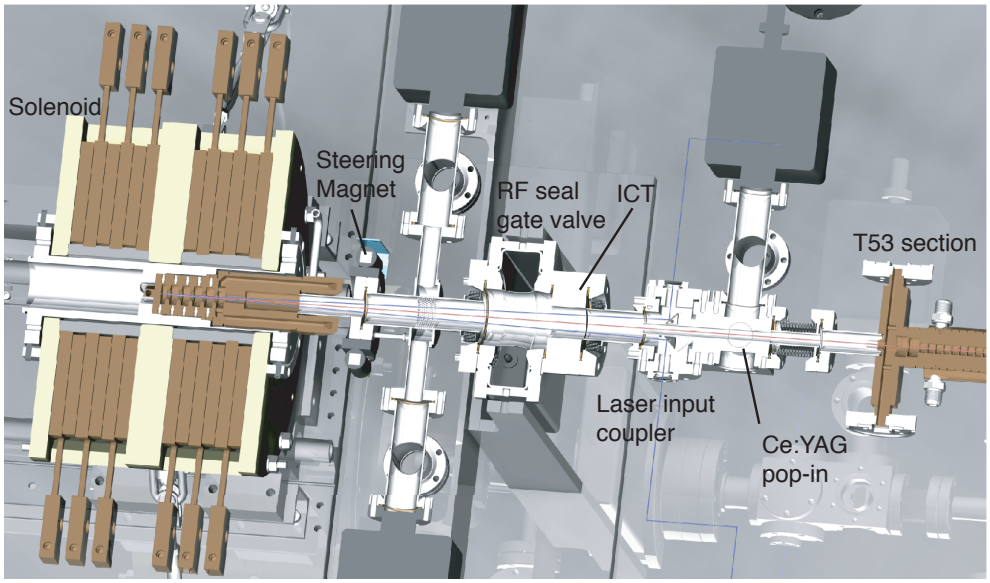

Figure 2. CAD rendering of VELOCIRAPTOR injector beamline.

The drift length from cathode to accelerator section is 80 cm. The UV laser is passed through a vacuum window and directed with a mirror toward the cathode at a 2° incidence angle. An additional diagnostic mirror is placed opposite the laser mirror with a beam tube located on-axis to minimize wakes. Diagnostics include an Integrating Current Transformer (ICT) to measure charge, and a Ce:YAG scintillator used to measure the beam size and profile. With the 80 cm drift length excellent electron beam quality is achieved, as shown in simulations below.

ACCELERATOR SECTIONS

The accelerator consists of the photo-gun and six sections of traveling wave accelerating structure, the T53. The T53 type traveling wave structure was extensively tested for high gradient operation and has operated at high gradient with low breakdown rates [9]. This structure, shown in figure 3, is suitable for our LINAC because our electron bunch separation is large enough (~10 ns) that wake-fields are not likely to degrade the electron beam quality from bunch to bunch. The T-series structures are essentially the low group velocity (downstream) portion of the original 1.8 m

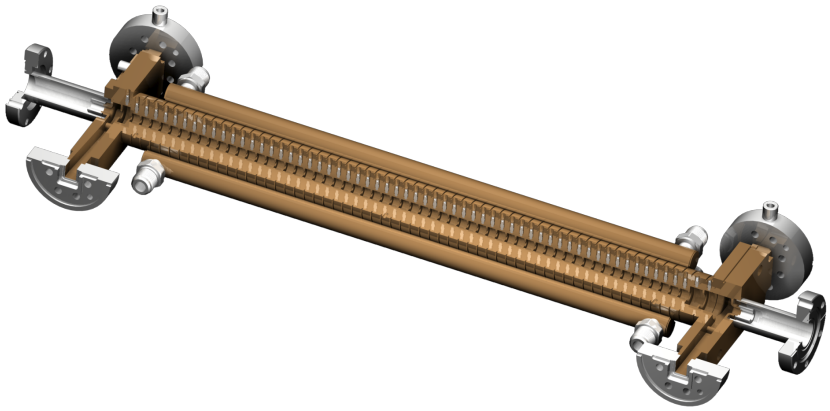

Figure 3. CAD rendering of the T53 accelerator section.

structures. This structure can be operated with acceptable trip rate at gradients up to 90 MV/m [9]. We plan to operate these sections at 70 MV/m.

Like the photoinjector, the T53 is a dual feed structure. If uncompensated, the rf quadrupole field in the coupling cells were found in simulations to produce a significant amount of emittance growth – up to 0.1 mm mrad. The input and output coupling cells have been redesigned to incorporated the racetrack geometry, which decreases the amplitude of the rf quadrupole by an order of magnitude.

RF POWER

X-band rf power will be supplied by XL-4 klystrons, developed by SLAC in the mid 90's for the high power testing of the X-band structures [16] for the Next Linear Collider program. The XL-4 is a solenoid focused klystron which requires a 0.47 Tesla solenoid, and produces 50MW of rf power in 1.5 msec pulses. A solid-state high voltage modulator provides the high voltage pulse required by the klystron. We have chosen the solid-state modulator (K2-3X) built by ScandiNova for its pulse-to-pulse stability and solid-state modular design. This modulator produces 450 kV, 350 Amp, 1.5 msec (duration of flat-top) pulses for the klystron at up to 120 Hz repetition rate. The pulse-to-pulse voltage jitter is expected to be approximately 0.1%, which is compatible with the 0.1% electron beam energy stability required by the γ–ray source. Two klystrons and two high voltage modulators are planned for VELOCIRAPTOR.

The peak rf power required by the gun and 6 accelerator section is approximately 450 MW for 210 ns (~3 fill times). To accomplish this, the 100 MW combined output of the klystrons is fed into a pulse compression system. SLAC has developed and demonstrated SLED II with multi-mode delayed lines with similar power gain factor [17]. The dual-mode SLED-II delay lines will be approximately 15 meter long with inner diameter of 17 cm.

The compressed rf pulses will be fed into a 13 dB coupler, diverting approximately 25MW to the rf gun. To allow for tuning and control, a phase shifter and attenuator are put in this arm. A barrier window is also planned for the rf gun. This is to limit the number of times the rf gun is exposed to air and to possibly provide for a configuration in which the rf gun can be baked and sealed as a unit

before installation. The rest of the compressed power is to be distributed to the linear accelerator sections. A 3 dB H-hybrid is used to divide the 425 MW in half. Then a combination of 4.8 dB and 3 dB H-hybrids are used to distribute the power to each T53 section. Phase shifters and other control elements will be added as needed.

BEAM TRANSPORT

The key issues addressed in the design of the beam transport lattice from the exit of the linac to the Compton scattering IP are emittance preservation, mitigation of on-axis Bremsstrahlung, and incorporation of the interaction laser into the final-focus optical system. In previous Compton source development work at LLNL, unwanted background radiation limited the utility of many of the γ–ray beam diagnostics employed. This radiation was observed to be effectively on-axis (i.e., only partially removed by collimation), unchanged by absence of photo-beam, and eliminated by removing rf power in the photo-gun. Spectral measurements were performed using a high-purity Germanium detector, which showed the radiation to be broadband, and extending upwards of 8 MeV (detector range limited). From this evidence, the noise source is determined to be Bremsstrahlung produced by dark current electrons generated in the gun and striking the walls of the accelerator and vacuum system downstream.

The increase in surface electric fields in the planned machine, and its associated increase in dark current, makes the removal of the anticipated on-axis Bremsstrahlung an important lattice design consideration. For this machine, the dog-leg and chicane geometries have been investigated [8]. Both the dog-leg and chicane beamlines offer methods to shield radiation on the linac axis, while terminating dispersion-free ($\eta = \eta' = 0$). While the dog-leg design offsets the γ–ray beam from the linac axis, and offers better potential for shielding, it is less compact, requires strong focusing, and is operationally less robust than the chicane. The chicane also has the advantage that it can be disabled to allow straight through operation if desired. While either lattice may be used for bunch compression, this design focuses on emittance preservation. The study described in Ref. [8] investigated the effect of coherent synchrotron radiation (CSR) on emittance in different dog-leg and chicane beamlines, and showed that CSR induced emittance growth could be kept negligible in the case of a small bend angle chicane.

The VELOCIRAPTOR transport line, shown in Fig. 4, features a four dipole chicane using 7°, 3 meter radius of curvature bends which shifts the electron beam 5 cm off-axis for Bremsstrahlung

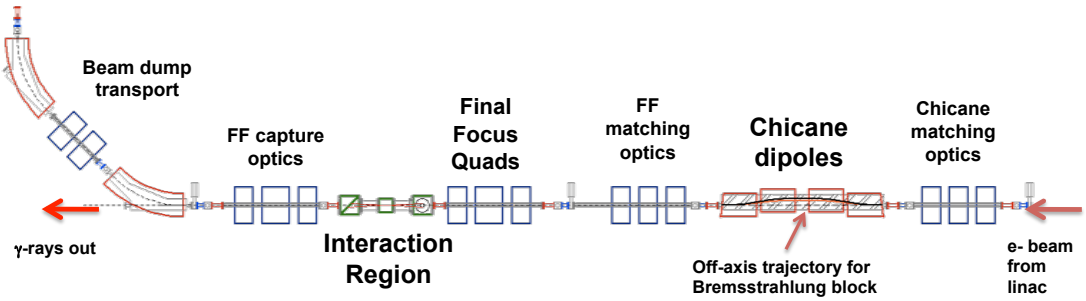

Figure 4. Schematic of the electron beam transport line, including a four dipole chicane that enables shielding of on-axis Bremsstrahlung, the Compton scattering interaction region, and beam dump.

shielding. In addition, quadrupole triplets are used to control the beam injected into the chicane, and to control both the beam size and divergence at the interaction point. VELOCIRAPTOR uses a 180° scattering geometry that passed the electron beam through holes in two mirrors used to bring the laser to the interaction point. This geometry permits the implementation of Recirculation Injection by Nonlinear Gating (RING) [18] in the future.

ACCELERATOR SIMULATIONS

The expected performance of the γ–ray source has been modeled using several different simulation codes. To model the electron beam from the photo-cathode through the linac the code PARMELA was used in the simulation results shown below. These results have been benchmarked against the codes GPT and ASTRA with good agreement found between the codes. To transport the beam through the bend magnets and focus at the interaction point including CSR effects, particle phase space distributions generated by PARMELA were input to the code ELEGANT. Finally, the output distribution from ELEGANT was used in a custom Compton scattering simulation code developed at LLNL and benchmarked against experimental data [19].

The choice of electron beam parameters for VELOCIRAPTOR is guided by scaling the beam dynamics from the so-called 'LCLS working point' design [20]. An initial set of parameters established by increasing the beam density to balance the increased focusing forces in the X-band accelerator was optimized in simulations incorporating the field maps for the VELOCIRAPTOR photo-gun, solenoid, and T-53 section. The optimized input parameters are given in Table 1.

Table 1. Parameters for VELOCIRAPTOR linac simulations

Parameter	Value
Gun peak field	200 MV/m
T-53 gradient	70 MV/m
Cathode to T-53 distance	80 cm
Charge	250 pC
Laser temporal	8x 200 fs FWHM, 275 fs spacing
Laser spatial	σ_r = 0.55 mm, r_{cut} = 0.46 mm
Intrinsic emittance	0.9 mm per mm
Final emittance (rms)	0.35 mm
Electron energy	250 MeV
Energy spread (rms)	0.17%

The peak accelerating field used in the photo-gun was based on the performance of the Vlieks gun. The T-53 accelerating gradient was set based on the expected amount of rf power delivered to each section. The simulations assume a cathode laser consisting of a train of 8 Gaussian pulses with temporal duration of 200 fs FWHM spaced by 275 fs. The resulting temporal profile is approximately 2 ps in duration with significant intensity variation between the stacked pulses. This variation could be reduced by decreasing the spacing between pulses, but was found to have a minimal effect on the beam projected emittance, and helps minimize the effect of misalignments of the Hyper-Michelson interferometer used to generate the pulse train. The laser pulses are Gaussian

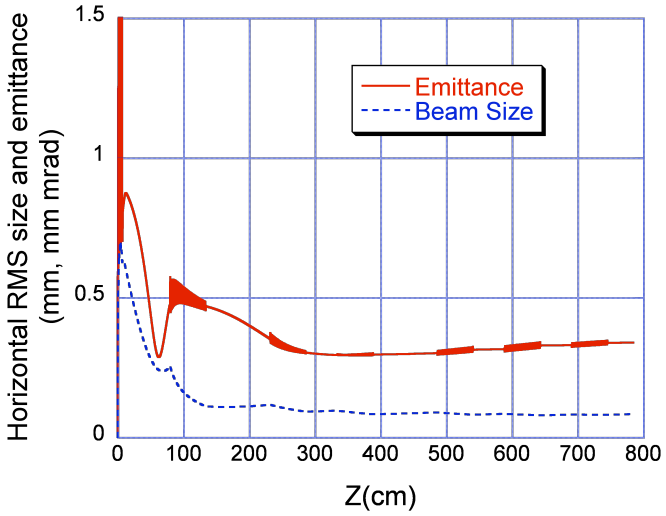

Figure 5. PARMELA simulation of the rms horizontal beam size and emittance in the VELOCIRAPTOR linac.

spatially with σ_r = 0.55 mm, but with a hard cut on the distribution at r = 0.46 mm — note that here σ_r represents the initial Gaussian σ, not the rms size of the clipped beam.

The simulated evolution of the horizontal rms size and emittance through the linac for the parameters in Table 1 are shown in Fig. 5. In this simulation there is a thermal distribution of velocities of the particles emitted from the cathode that corresponds to an intrinsic emittance of 0.9 mm, rms per mm of laser spot radius. As the figure shows, the horizontal emittance reaches a minimum value after roughly 2 T-53 sections of 0.35 mm, rms. The beam transport system allows flexibility in the choice of final focus electron beam size. The MEGa-ray source application needs must be used to determine the relative importance of bandwidth and total flux. Here, consider the example in which the electron beam focusing is chosen such that the effect on γ source bandwidth is

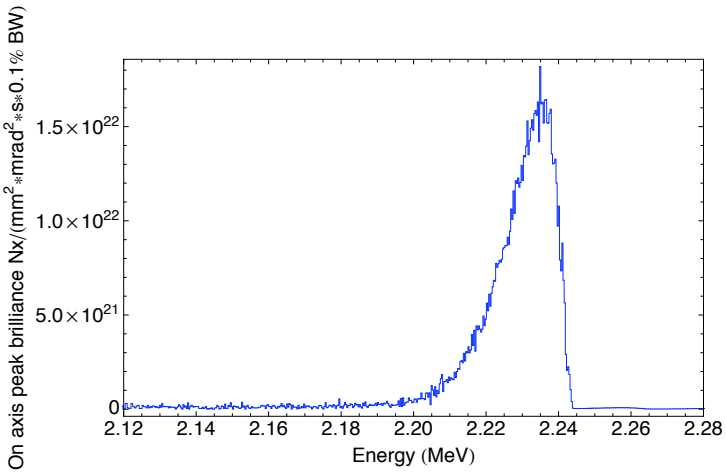

Figure 6. Simulated on-axis gamma-ray spectrum produced by the beam parameters in Table 1.

comparable to that of energy spread — $\varepsilon_x^2/\sigma_x^2$ = 0.2%. If the interaction laser spot size is matched to that of the electron beam in this simulation, and the laser intensity is kept low enough to make nonlinear effects negligible, the simulated on-axis spectrum generated is shown in Fig. 6. In this simulation the on-axis bandwidth is < 1% while the total photon flux is 8×10^7 per shot.

CONCLUSIONS

The VELOCIRAPTOR linac has been designed as a driver for a compact, high brightness, precision MEGa-ray source. The longitudinal and transverse beam dynamics of the X-band photoinjector have been studied in order to choose an operating parameter set that maximizes the average brightness, $\langle I \rangle / \varepsilon_n^2$, given the expected performance of the rf accelerator. The design is made possible by linear collider driven development of X-band rf power and accelerator technologies.

The MEGa-ray source driven by VELOCIRAPTOR is predicted to approach 400 photons/eV/sec when operated at 120 Hz repetition rate, with planned future upgrades using the RING technology and micro-bunched electron beams to increase the flux by 2 orders of magnitude. These levels of brilliance in the MeV regime will enable a variety of NRF-based isotope-specific applications. VELOCIRAPTOR is designed for flexibility to meet varying application needs, with ongoing research focused on methods to minimize bandwidth or maximize total flux.

This work was performed under the auspices of the U.S. Department of Energy by Lawrence Livermore National Laboratory under Contract DE-AC52-07NA27344.

REFERENCES

1. U. Kneissl, H. M. Pitz, A. Zilges, *Prog. Part. Nucl. Phys.,* **37** p. 349-433 (1996).
2. W.Bertozzi, *et al.*, *Phys. Rev. C,* **78** 041601 (2008).
3. C.A. Hagmann, *et al.*, *J. Appl. Phys.,* **106** 084901 (2009).
4. N. Kikuzawa, *et al.*, *Appl. Phys. Express*, **2** 036502 (2009).
5. F. Albert, *et al*., *Opt. Lett.*, **35** p. 354 (2010).
6. D.J. Gibson, *et al.*, *Phys. Rev. ST – Accel. Beams*, **13** 070703 (2010).
7. F. Albert, *et al.*, *Phys. Rev. ST – Accel. Beams*, **13** 070704 (2010).
8. S.G. Anderson, *et al., Proc. of PAC09*, p. 1186 (2009).
9. C. Adolphsen, *Proc. of PAC03*, p. 668 (2003).
10. A.E. Vlieks, *et al.*, *Proc. of High Energy Density and High Power RF: 5th Workshop*, **CP625**, AIP, p.107 (2002).
11. A.E. Vlieks, *et al.*, *Proc. of High Energy Density and High Power RF: 6th Workshop*, **CP691**, AIP, p.358 (2003).
12. R.A. Marsh, *et al., Phys. Rev. ST – Accel. Beams, in Preparation*.
13. See *http://www.slac.stanford.edu/grp/acd/ace3p.html*.
14. O. A. Nezhevenko, *Proc. of PAC97*, p. 3013, (1997).
15. L. Xiao, R. Boyce, D. Dowell, Z. Li, C. Limborg-Deprey, J. F. Schmerge, *Proc. of PAC05*, p. 3432 (2005).
16. G. Caryotakis, Presented at *3rd International Workshop on RF Pulsed Power Sources for Linear Colliders (RF 96)*, Hayama, Japan, (1996).
17. S.G. Tantawi, *et al*., *Phys. Rev. ST – Accel. Beams*, **8** 042002 (2005).
18. I. Jovanovic, *et al., Proc. of PAC07*, p. 1251 (2007).

19. W.J. Brown, *et al., Phys. Rev. ST – Accel. Beams*, **7** 060702 (2004).
20. M. Ferrario, *et al., Proc. of ICFA Advanced Accelerator Workshop on the Physics of High Brightness Beams*, p. 534 (2000).